Appendix D:

Lin, K.-C. and Faeth, G.M. (2000) "State Relationships of Laminar Permanently-Blue Opposed-Jet Hydrocarbon-Fueled Diffusion Flames," *Int. J. Environ. Combust. Tech.* 1, 53-79.

Environ Comb Tech, Vol 1, pp 53–79
Reprints available directly from the publisher
Photocopying permitted by license only

State Relationships of Laminar Permanently-Blue Opposed-Jet Hydrocarbon-Fueled Diffusion Flames

K.-C. LIN and G. M. FAETH*

Department of Aerospace Engineering, The University of Michigan, Ann Arbor, Michigan 48109-2140, U.S.A.

(Received August 1997; Revised November 1998)

The structure and state relationships of laminar soot-free (permanently-blue) diffusion flames at various strain rates were studied experimentally using an opposed-jet configuration, motivated by the importance of soot-free hydrocarbon-fueled diffusion flames for many practical applications. Measurements of gas velocities, temperatures and compositions were carried out along the stagnation stream line. Flame conditions studied included propylene- and 1,3-butadiene-fueled opposed-jet diffusion flames having a stoichiometric mixture fractions of 0.7 and strain rates of 60–240 s^{-1} at normal temperature and pressure. It was found that oxygen leakage to fuel-rich conditions and carbon monoxide leakage to fuel-lean conditions both increased as strain rates increased. Furthermore, increased strain rates caused increased fuel concentrations near the flame sheet, decreased peak gas temperatures, and decreased concentrations of carbon dioxide and water vapor throughout the flames. State relationships for major gas species and gas temperatures for these flames were found to exist over broad ranges of strain rates. In addition, current measurements, as well as previous measurements and predictions of ethylene-fueled permanently-blue diffusion flames, all having a stoichiometric mixture fraction of 0.7, were combined to establish generalized state relationships for permanently-blue diffusion flames for this stoichiometric mixture fraction. The combined measurements and predictions support relatively universal generalized state relationships for N_2, CO_2, H_2O and fuel over a broad range of strain rates and fuel types. State relationships for O_2 in the fuel-rich region, and for CO in the fuel-lean region, however, are functions of strain rate and fuel type. State relationships for H_2 and temperature exhibit less universality, mainly due to the increased experimental

* Tel: 734-764-7202; Fax: 734-936-0106; E-mail: gmfaeth@umich.edu

uncertainties for these variables. The existence of state relationships for soot-free hydrocarbon-fueled diffusion flames provides potential for significant computational simplifications for modeling purposes in many instances, allowing for effects of finite-rate chemistry while avoiding time-consuming computations of Arrhenius expressions.

Keywords: Laminar flames; soot control; diffusion flames; hydrocarbon flames

INTRODUCTION

Soot-free hydrocarbon-fueled diffusion flames are of significant interest because many practical combustion processes achieve this condition in order to avoid soot emissions. In addition to their practical importance, however, soot-free diffusion flames created by available soot control methods provide an ideal environment for studies of flame structure and modeling because they avoid complications caused by the presence of soot (Lin and Faeth, 1998). These complications include continuum radiation heat transfer to the environment from soot, difficulties with measurements due to the deposition of soot on probes, and complex coupling between soot formation mechanisms and much simpler purely gas phase reaction processes. Previous work (Lin and Faeth, 1996a,b; Du and Axelbaum, 1995; Sugiyama, 1994) has shown that soot-free diffusion flames can be obtained using fast mixing concepts that reduce the residence times of fuel and fuel decomposition species at fuel-rich conditions which limits the formation of soot precursors and soot so that these materials can be oxidized completely when they pass into the fuel-lean portions of the flames. In addition to conventional use of intense combustion processes, appropriate mixing can be enhanced by controlling flow velocities normal to the flame sheet so that they are more directed from the fuel-rich to the fuel-lean side, which intrinsically reduces fuel residence times at fuel-rich conditions (Lin and Faeth, 1996a,b). In fact, such tactics can provide soot-free hydrocarbon-fueled diffusion flames, or permanently-blue flames, for flame strain rates extending from nearly zero up to extinction conditions (Lin and Faeth, 1996b, 1998). One approach to achieve soot-free flames in this way has been achieved by controlling the stoichiometric mixture fraction (Lin and Faeth, 1996b; Du and Axelbaum, 1995), which changes the flow velocities normal to the flame sheet and flame compositions; another approach involves controlling strain rates (Lin and Faeth, 1996b), which reduces the soot formation regions by reducing the residence times in chemical reaction zones. Both tactics can be applied to the opposed-jet configuration which has received much attention for studies of both flame structure and modeling (Lin and Faeth, 1998; Sun *et al.*, 1996).

Previous studies of permanently-blue ethylene-fueled opposed-jet diffusion flames have shown that these flames can be simulated reasonably well over a broad range of strain rates using available chemical reaction mechanisms (Lin and Faeth, 1998). Furthermore, it was found that state relationships for these ethylene-fueled permanently-blue diffusion flames exist for major gas species concentrations and temperature. State relationships offer a promising approach to analyze turbulent diffusion flames in conjunction with the conserved scalar formalism, where data from laminar diffusion flames is used to simulate corresponding turbulent diffusion flames (Bilger, 1976, 1977). The main advantage of this approach is that computationally intensive reaction rate calculations involving Arrhenius expressions are avoided while still providing a realistic estimate of composition and temperature distributions in the flow. However, findings for simple ethylene-fueled diffusion flames still cannot be applied to practical hydrocarbon combustion processes that involve complex interactions between strain rates and fuel-decomposition processes. Therefore, it is desirable to extend the earlier study of ethylene-fueled diffusion flames to consider measurements of flame structure for other hydrocarbon-fueled diffusion flames, in order to establish the potential for simplified modeling of practical hydrocarbon-fueled turbulent diffusion flames.

It is also of interest to study whether generalized state relationships exist for hydrocarbon-fueled diffusion flames at different levels of strain. Several studies, such as Mitchell *et al.* (1980), Smyth *et al.* (1985), and Saito *et al.* (1986), tried to establish state relationships for major gas species based on measurements of soot-containing methane/air diffusion flames. Their results are not particular satisfactory for the fuel-rich regions, probably due to the presence of soot inside the flames. Sivathanu and Faeth (1990) also tried to established generalized state relationships for major gas species based on available experimental data for hydrocarbon-fueled flames, ranging from methane to n-heptane. Once again, significant departures from equilibrium predictions were observed at fuel-rich conditions. Whether the presence of soot, or finite rate chemistry, causes these departures from equilibrium predictions can be examined by studying the state relationships of soot-free diffusion flames. Thus, the correlations originally developed by Sivathanu and Faeth (1990), with some necessary modifications, will be used to examine the existence of generalized state relationships for soot-free hydrocarbon-fueled diffusion flames.

In view of the previous observations, the overall objectives of the present study are to extend the work of Lin and Faeth (1998) in order to gain a better understanding of hydrocarbon-fueled diffusion flames for soot-free conditions, emphasizing the potential existence of state relationships to correlate scalar properties within them. The specific objectives of the study can be summarized as follows:

1. Study the structure of permanently-blue propylene- and 1,3-butadiene-fueled opposed-jet diffusion flames, emphasizing a range of strain rates in order to highlight potential effects of finite-rate chemical reactions on flame structure.
2. Investigate whether state relationships exist for these permanently-blue flames over the available range of strain rates.
3. To establish whether generalized state relationships exist for permanently-blue hydrocarbon-fueled flames having a given stoichiometric mixture fraction (0.7 for present conditions) for the available range of fuel types and strain rates.

The discussion begins with consideration of the theoretical basis for generalized state relationships. This is followed by a description of the experimental methods. Results are then considered, treating flame structure, state relationships for each fuel and generalized state relationships for permanently-blue hydrocarbon-fueled flames, in turn.

THEORETICAL BASIS FOR GENERALIZED STATE RELATIONSHIPS

Sivathanu and Faeth (1990) have developed a set of generalized state relationships for the major gas species within hydrocarbon/air diffusion flames burning at normal temperature and pressure. The hypothesis used to develop these correlations is that effects of H/C ratio should scale in the same manner for fuel-lean conditions because the properties of this region either are primarily controlled by passive mixing or exhibit a type of quasi-equilibrium that appears to be related to species concentrations at the stoichiometric mixture ratio. Then since permanently-blue flames can be created in such a way that the molar flow ratios of fuel, oxygen and nitrogen are the same as the pure fuel burning in the ambient air (Lin and Faeth, 1996b, 1998; Du and Axelbaum, 1995), these earlier correlations for hydrocarbon/air diffusion flames can be used for permanently-blue diffusion flames with only some modest modifications.

Following the work of Sivathanu and Faeth (1990), a mixture of nitrogen and a general hydrocarbon, C_nH_m, reacting with an oxygen-nitrogen mixture to yield saturated combustion products at lean conditions, has the following stoichiometry on a per mole of fuel basis:

$$(C_nH_m + aN_2) + \chi[(n + m/4)O_2 + bN_2] \rightarrow nCO_2 + (m/2)H_2O$$
$$+ (n + m/4)(\chi - 1)O_2 + (a + b\chi)N_2 \quad (1)$$

where a and b are the number of moles of N_2 per mole of fuel in the fuel and oxidizer streams, respectively, and χ is the molal oxidizer-stream to fuel-stream flow rate ratio and is equal to unity at the stoichiometric condition. The values of a and b are adjusted in such a way that a permanently-blue flame is created while the molar ratios of fuel, oxygen and nitrogen are kept the same as that of the pure fuel burning in the dry ambient air with a specific stoichiometric mixture fraction, Z_{st} at stoichiometric condition. The relationship between a, b and Z_{st} can be expressed as follows:

$$a + b = (n + m/4)k \quad (2)$$

and

$$a = (Z_{st}M_{react} - M_f)/M_{N_2} \quad (3)$$

where k is the number of moles of N_2 per mole of O_2 in the air ($k = 3.76$ for dry ambient air). The mass fraction, Y_i, for any species appearing on the right-hand side of Equation 1 can be found from the following expression:

$$Y_i = \nu_i M_i/[M_f + (n + m/4)\chi M_{O_2} + (a + b\chi)M_{N_2}] \quad (4)$$

where ν_i is the number of moles of a product species, i, per mole of fuel (e.g., $\nu_{CO_2} = n$), M_i is the molecular weight of species i, and the subscript f denotes the fuel. The fuel-stream to oxidizer-stream mass ratio, f, in Equation 1 can be found from the following expression:

$$f = (M_f + aM_{N_2})/\chi[(n + m/4)M_{O_2} + bM_{N_2}] \quad (5)$$

Finally, the fuel-equivalence ratio, ϕ, is defined as follows:

$$\phi = f/f_s \tag{6}$$

where the subscript s denotes a quantity at the stoichiometric condition.

Substituting Equations 5 and 6 into Equation 1, and using boundary and stoichiometric conditions to simplify the expression, yields the following relationships between ϕ and the mass fraction of oxygen:

$$1 - \phi = \left(\frac{\left(n + \frac{m}{4}\right) M_{O_2} + (M_f + aM_{N_2}) Y_{O_2,O}}{\left(n + \frac{m}{4}\right) M_{O_2} + (M_f + aM_{N_2}) Y_{O_2}} \right) \left(\frac{Y_{O_2}}{Y_{O_2,O}} \right) = \psi_{O_2} \tag{7}$$

where the subscript O denotes a boundary oxidizer-stream condition. This function was used to plot the generalized state relationship for the mass fraction of oxygen. In arriving at Equation 7 for ψ_{O_2}, $Y_{O_2,S} = 0$ has been used, this is not strictly true but is a reasonable approximation for combustion of hydrocarbons in air. Finally, $1 - \phi$ appears on the left-hand side of Equation 7 for convenience in plotting the state relationship.

The generalized state relationship functions for the mass fractions of carbon dioxide and water vapor can be found in the same manner, as follows:

$$\phi = \left(\frac{nM_{CO_2} - (M_f + aM_{N_2}) Y_{CO_2,S}}{nM_{CO_2} - (M_f + aM_{N_2}) Y_{CO_2}} \right) \left(\frac{Y_{CO_2}}{Y_{CO_2,S}} \right) = \psi_{CO_2} \tag{8}$$

and

$$\phi = \left(\frac{\left(\frac{m}{2}\right) M_{H_2O} - (M_f + aM_{N_2}) Y_{H_2O,S}}{\left(\frac{m}{2}\right) M_{H_2O} - (M_f + aM_{N_2}) Y_{H_2O}} \right) \left(\frac{Y_{H_2O}}{Y_{H_2O,S}} \right) = \psi_{H_2O} \tag{9}$$

The mass fractions of carbon dioxide and water vapor at stoichiometric conditions can be obtained from Equations 1 and 4.

The generalized state relationship for nitrogen is simply defined as the normalization of mass fraction of nitrogen, using the boundary conditions at the fuel and oxidizer streams, as follows:

$$\psi_{N_2} = \left(\frac{Y_{N_2} - Y_{N_2,O}}{Y_{N_2,F} - Y_{N_2,O}} \right) \tag{10}$$

where F and O denote the initial property at the fuel and oxidizer streams, respectively. This definition is based on the fact that nitrogen is relatively nonreactive in typical hydrocarbon combustion processes.

Equation 1 cannot be used for fuel-rich conditions during the development of the generalized state relationship correlations for species concentrations, because stoichiometry assuming only the presence of saturated combustion products is no longer appropriate. Therefore, the state relationship for fuel was obtained using the fuel-stream boundary condition to normalize the mass fraction of fuel, as follows:

$$\psi_f = Y_f / Y_{f,F} \tag{11}$$

The corresponding relationships for carbon monoxide and hydrogen were obtained by assuming that Y_{CO} was analogous to Y_{CO_2} in Equation 8, and that Y_{H_2} was analogous to Y_{H_2O} in Equation 9, yielding the following functions:

$$\psi_{CO} = \left(\frac{nM_{CO_2} - (M_f + aM_{N_2})Y_{CO_2,S}}{nM_{CO_2} - (M_f + aM_{N_2})Y_{CO}} \right) \left(\frac{Y_{CO}}{Y_{CO_2,S}} \right) \tag{12}$$

and

$$\psi_{H_2} = \left(\frac{\left(\frac{m}{2}\right) M_{H_2O} - (M_f + aM_{N_2})Y_{H_2O,S}}{\left(\frac{m}{2}\right) M_{H_2O} - (M_f + aM_{N_2})Y_{H_2}} \right) \left(\frac{Y_{H_2}}{Y_{H_2O,S}} \right) \tag{13}$$

Finally, the generalized state relationship functions for permanently-blue hydrocarbon-fueled diffusion flames are summarized in Table I.

EXPERIMENTAL METHODS

Apparatus

The present measurements were carried out using a laminar opposed-jet diffusion flame apparatus similar to Lin and Faeth (1998), which will only be described briefly here. A stable, plane flame was established at the middle of the 8-mm-wide gap between the exits of the upper and lower burner tubes, by adjusting the momentum of the fuel and oxidizer streams. Fuel and nitrogen were supplied through the inner tube of the lower part of the burner while oxygen and nitrogen were supplied through

TABLE I Generalized State Relationship Functions

Species i	ψ_i
N_2	$\left(\dfrac{Y_{N_2} - Y_{N_2,O}}{Y_{N_2,F} - Y_{N_2,O}}\right)$
O_2	$\left(\dfrac{\left(n + \frac{m}{4}\right) M_{O_2} + (M_f + aM_{N_2})Y_{O_2,O}}{\left(n + \frac{m}{4}\right) M_{O_2} + (M_f + aM_{N_2})Y_{O_2}}\right)\left(\dfrac{Y_{O_2}}{Y_{O_2,O}}\right)$
C_nH_m	$\left(\dfrac{Y_f}{Y_{f,F}}\right)$
CO_2	$\left(\dfrac{nM_{CO_2} - (M_f + aM_{N_2})Y_{CO_2,S}}{nM_{CO_2} - (M_f + aM_{N_2})Y_{CO_2}}\right)\left(\dfrac{Y_{CO_2}}{Y_{CO_2,S}}\right)$
H_2O	$\left(\dfrac{\left(\frac{m}{2}\right) M_{H_2O} - (M_f + aM_{N_2})Y_{H_2O,S}}{\left(\frac{m}{2}\right) M_{H_2O} - (M_f + aM_{N_2})Y_{H_2O}}\right)\left(\dfrac{Y_{H_2O}}{Y_{H_2O,S}}\right)$
CO	$\left(\dfrac{nM_{CO_2} - (M_f + aM_{N_2})Y_{CO_2,S}}{nM_{CO_2} - (M_f + aM_{N_2})Y_{CO}}\right)\left(\dfrac{Y_{CO}}{Y_{CO_2,S}}\right)$
H_2	$\left(\dfrac{\left(\frac{m}{2}\right) M_{H_2O} - (M_f + aM_{N_2})Y_{H_2O,S}}{\left(\frac{m}{2}\right) M_{H_2O} - (M_f + aM_{N_2})Y_{H_2}}\right)\left(\dfrac{Y_{H_2}}{Y_{H_2O,S}}\right)$

the inner tube of the upper part of the burner; both these tubes had an inside diameter of 10.3 mm, a wall thickness of 0.4 mm, and a passage length of 200 mm. Annular coflowing streams of nitrogen surrounding both the fuel and oxidizer streams were introduced through outer tubes having an inside diameter of 18.3 mm and a wall thickness of 0.4 mm. The objective of the coflowing streams was to eliminate oxidizer entrainment and to minimize disturbances from the surrounding environment. Two honeycomb sections (cell sizes of 1.6 mm and lengths of 25 mm) were located 70 and 140 mm from the exit of each inner burner tube to smooth the velocity profiles leaving these tubes. The entire burner assembly could be traversed in the vertical and horizontal directions using stepping-motor-driven linear positioners (having a 5-μm positioning accuracy in each direction) to accommodate rigidly-mounted optical instrumentation.

Fuel, oxygen and nitrogen were supplied from commercial gas cylinders. The gas flows were controlled by pressure regulators and were measured using rotameters that were calibrated using either bubble flow meters or wet-test meters.

Instrumentation

Velocities were measured by laser velocimetry based on a dual-beam forward-scattering arrangement, with the flow seeded with aluminum oxide particles whose nominal diameter was 1 μm, similar to past work (Lin, 1996; Lin and Faeth, 1996a, b, 1998; Lin *et al.*, 1996; Sunderland and Faeth, 1995). An argon-ion laser operating at a wave length of 514.5 nm, with an optical power of 300 mW, was used as the coherent light source. In order to increase the spatial resolution of the probe volume for the narrow gaps of opposed-jet burners, a beam expander having an expansion ratio of 3.75 was used to provide a relatively small measuring volume (diameter of roughly 60 μm and length of roughly 410 μm). The detector output was amplified and processed using a burst counter signal processor. The low-pass filtered analog output of the signal processor was sampled at equal time intervals using a lock-in amplifier. A personal computer was used to collect the data. Experimental uncertainties (95% confidence) of the streamwise velocities generally were less than 3%, dominated by calibration uncertainties.

Temperature profiles along the flame axes were measured using Pt/Pt-10%Rh thermocouples having different bead diameters (Lin, 1996). The radiative emissivity and convective heat transfer rates of thermocouple beads are unknown; therefore, the proper radiation correction needed to find the true gas temperature is not known *a priori*. Furthermore, the bead geometry (which is usually assumed to be spherical by most of investigators) is complicated due to welding variations of the two dissimilar wire materials. Finally, the gas flow velocity field and several local gas properties are also needed in order to calculate the convective heat transfer coefficient to the thermocouple bead. All these effects create considerable uncertainties about corrections of thermocouple readings for effects of radiative heat losses.

In view of these problems, the present temperature measurements did not involve predictions of radiation corrections in order to estimate true gas temperatures. Instead, three thermocouples having different bead diameters (in the range 80–280 μm) were used to measure flame temperatures. The true gas temperatures were then found by extrapolating the uncorrected flame temperatures to a bead diameter of zero at each location. The bead diameter of each thermocouple needed for this procedure was measured using a comparator. The locations of the thermocouples were determined using a cathetometer having a reading accuracy of 10 μm. The output of the thermocouples was recorded using LabPac system installed on a personal computer. Experimental uncertainties (95% confidence) of the thermocouple temperature measurements were estimated to be less than 5%, dominated by the relocation uncertainties of the thermocouples and the uncertainties of measurements of bead diameters.

Stable gas species concentrations inside the permanently-blue flames were found by sampling the gas mixture with a microprobe and then analyzing the sample using gas chromatography (GC), similar to earlier work (Lin, 1995; Lin and Faeth, 1996a, b, 1998; Sunderland *et al.*, 1995). The quartz microprobe was constructed following Fristrom and Westenberg (1965); it had an inside diameter of 150 μm, an outside diameter of 250 μm at the tip, and was positioned horizontally in the flame. The location of the tip of the probe was determined using a cathetometer having a reading accuracy of 10 μm.

The water vapor within the flame degrades the performance of chromatograph columns. Therefore, a water-trap system filled with anhydrous calcium was installed just downstream of the microprobe to absorb the water vapor. The H_2O concentrations inside the propylene and 1,3-butadiene flames were calculated based on the assumption that the C/H molar ratio was preserved throughout the flame. Recent work suggests that this approach is problematical due to preferential diffusion of light hydrogen-containing species (Lin and Faeth, 1998); however, in the absence of detailed predictions of effects of preferential diffusion, correlations for these effects were not feasible.

The details of the GC arrangement for present measurements are presented by Lin (1996). The gas analysis system was calibrated with gas mixtures having known concentrations of the gaseous species to be measured. Experimental uncertainties (95% confidence) of gas concentration measurements are estimated to be less than 10%; the measurements were repeatable within this range during the course of testing.

Test Conditions

The test conditions are summarized in Table II. Propylene and 1,3-butadiene burning at atmospheric pressure were selected as the test fuels. Earlier results for ethylene-fueled flames from Lin and Faeth (1998) were used to supplement these results in order to find generalized state

TABLE II Test Conditions for Permanently-Blue Diffusion Flames*

Fuel†	*Molar Stoichiometry*‡ *Fuel/O_2/N_2*	*N_2 in Fuel (Vol. %)*	*N_2 in O_2 (Vol. %)*	*Strain Rate (s^{-1})*¶
C_2H_4	1.0/3.0/11.3	90.9	30.1	60, 120, 240
C_3H_6	1.0/4.5/16.9	93.8	30.0	60, 120, 200§
C_4H_6	1.0/5.5/20.7	94.8	30.3	60, 120, 240

*Laminar opposed-jet diffusion flames with an 8.0 mm gap, 10.3 mm inside diameter reactant ports, surrounded by 18.3 mm inside diameter coflowing nitrogen shroud flows, operating at atmospheric pressure with a stoichiometric mixture fraction of 0.7,

†Gas purities were as follows C_2H_4, 99.5%; C_3H_6, 99.0%, C_4H_6, 99.0%; oxygen, 99.5%, and nitrogen, 99.98%;

‡The stoichiometric molar ratio of fuel, oxygen and nitrogen is equivalent to that of pure fuel burning in the air,

¶Based on the correlation of Seshadri and Williams (1978),

§A stable and flat C_3H_6 flame having a strain rate of 240 s^{-1} could not be established.

relationships. Similar to Lin and Faeth (1998), the molar ratios of fuel, oxygen and nitrogen were kept the same as that of the pure fuel burning in the air while the stoichiometric mixture fraction, Z_{st}, was adjusted to be 0.7, in order to provide permanently-blue flames for all the test fuels. This condition was achieved by adding nitrogen to the fuel stream while increasing the oxygen concentration of the oxidizer stream (Du and Axelbaum, 1995; Lin and Faeth, 1996b, 1998). A stable, plane flame was established at the middle of the gap between the exits of the upper and lower tubes by adjusting the momentum of the fuel and oxidizer streams. Three strain rates (roughly 60, 120 and 240 s^{-1}) were considered in order to achieve a four-to-one variation of the strain rate so that effects of strain rates on flame structure and state relationships could be assessed. The upper bound of the strain rate was limited by the appearance of wrinkled flame surfaces while the lower bound of the strain rate was limited by conduction heat transfer losses to the burner ports.

RESULTS AND DISCUSSION

Flame Structure

Detailed flame structure measurements were undertaken for permanently-blue propylene-fueled opposed-jet diffusion flames having Z_{st} of 0.7. The

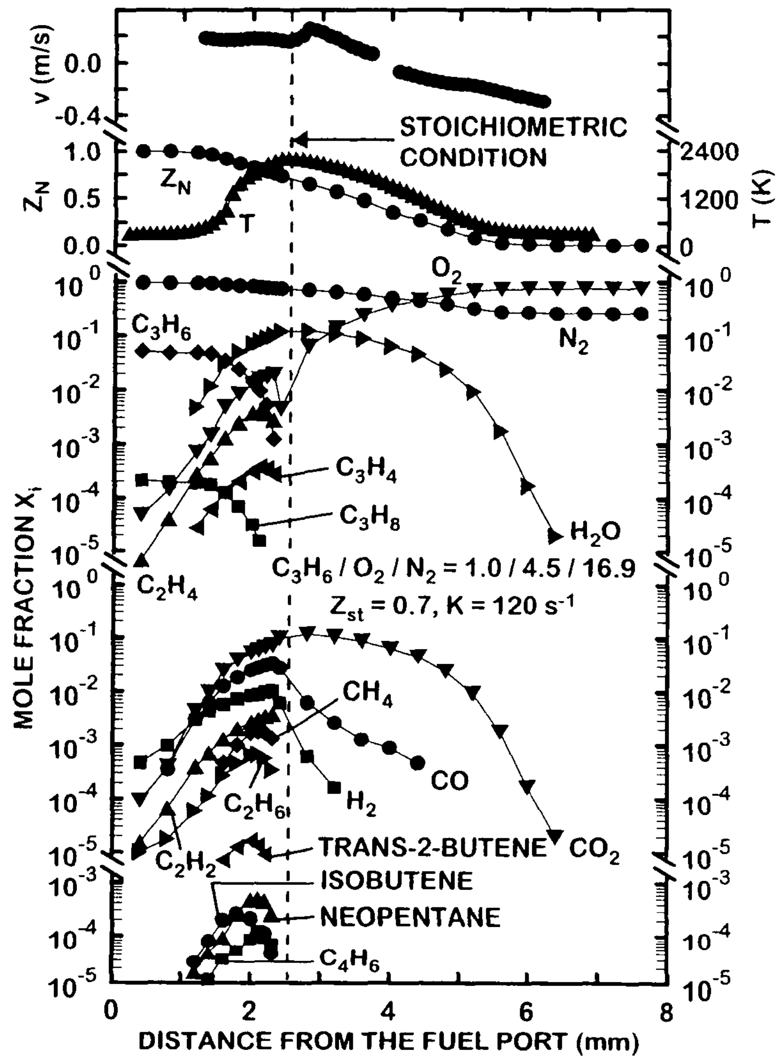

FIGURE 1 Measured velocities, temperatures and gas species concentrations in a permanently-blue, propylene-fueled, diffusion flame at a strain rate of 120 s^{-1}.

gas velocity, temperature, mixture fraction and gas species concentration distributions along the stagnation stream line of the flame having a strain rate of 120 s^{-1} are illustrated in Figure 1. Corresponding results for the propylene flames having strain rates of 60 and 200 s^{-1} are similar to Figure 1 and can be found in Lin (1996). The locations of the peak gas temperatures and concentrations of major combustion products, H_2O and CO_2, coincide with the flame sheet location based on the mixture fractions for each flame. The values of mixture fractions were calculated based on the nitrogen concentration to avoid problems of preferential-diffusion effects mentioned earlier (Lin and Faeth, 1997). Oxygen leaks through the flame sheet into the fuel-rich region, which assists the oxidation of soot precursors, similar to earlier observations for other permanently-blue diffusion flames (Lin and Faeth, 1998). Also, hydrogen and carbon monoxide penetrate into the fuel-lean region due to preferential-diffusion effects and finite-rate chemistry. Intermediate fuel decomposition species, ranging from CH_4 up to C_5 hydrocarbons, were detected in the fuel-rich region, however, these species are completely consumed before reaching the flame sheet. The peak gas temperatures and major gas species concentrations were roughly the same for all strain rates, considering experimental uncertainties; this behavior suggests the possible existence of state relationships for scalar properties for the permanently-blue propylene-fueled diffusion flames over the present strain rate test range. Similar to the earlier measurements of permanently-blue ethylene-fueled diffusion flames of Lin and Faeth (1998), increasing the strain rate over the present test range tends to reduce the width of the region containing combustion products. Finally, the water vapor concentrations illustrated in Figure 1 were calculated based on the assumption that the C/H molar ratio was constant throughout the flame because the predictions of the C/H molar ratio allowing for preferential diffusion were not available as noted earlier. Recent experience with this approximation suggests that C/H ratios are increased in the high temperature regions of the flames, tending to reduce water vapor concentrations from current estimates (Lin and Faeth, 1998).

In order to examine the potential existence of state relationships, and to provide measurements for future flame structure modeling evaluations for larger hydrocarbon species, the flame structure of the permanently-blue, 1,3-butadiene-fueled, opposed-jet diffusion flames were investigated along the stagnation stream line for strain rates of 60, 120 and 240 s^{-1}. The measured distributions of gas velocities, temperatures and major species concentrations for the flame having a strain rate of 240 s^{-1} are illustrated in Figure 2; the corresponding distributions of minor gas species concentrations for the same flame are illustrated in Figure 3. The

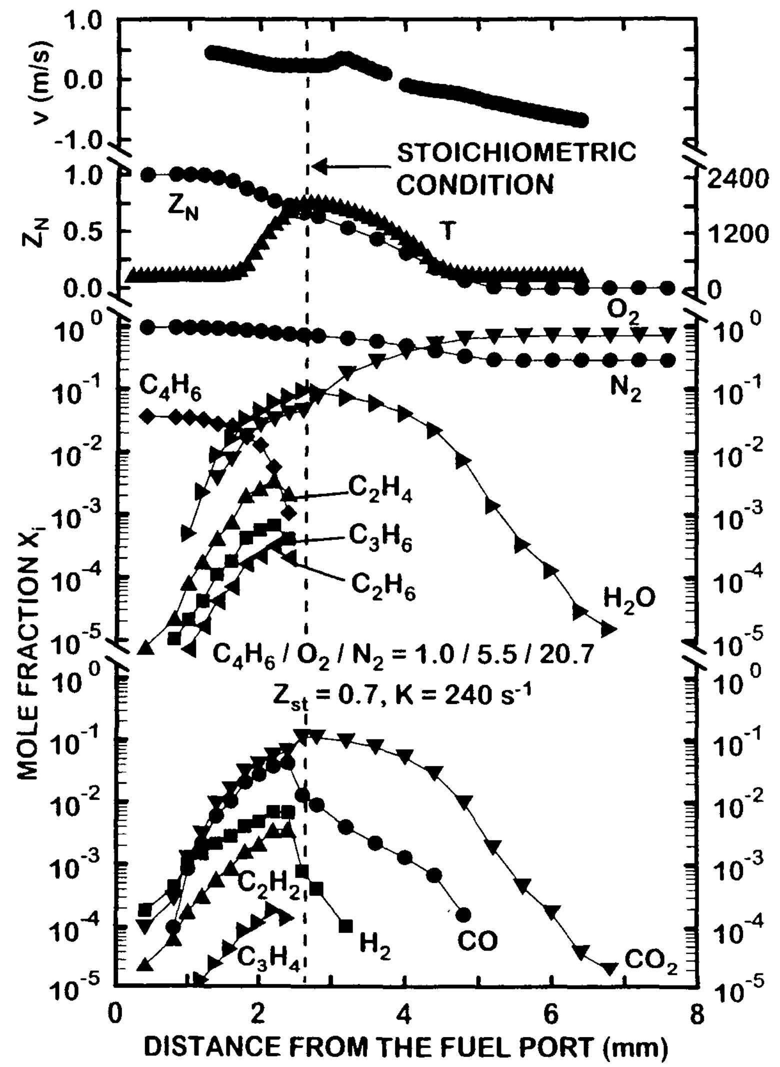

FIGURE 2 Measured velocities, temperatures and major gas species concentrations in a permanently-blue, 1,3-butadiene-fueled, diffusion flame at a strain rate of 240 s^{-1}.

structure of these flames for strain rates of 60 and 120 s^{-1} are similar (Lin, 1996). The general features of the structure of these flames are similar to the permanently-blue ethylene- and propylene-fueled diffusion flames discussed earlier (Lin, 1996; Lin and Faeth, 1998). Notably,

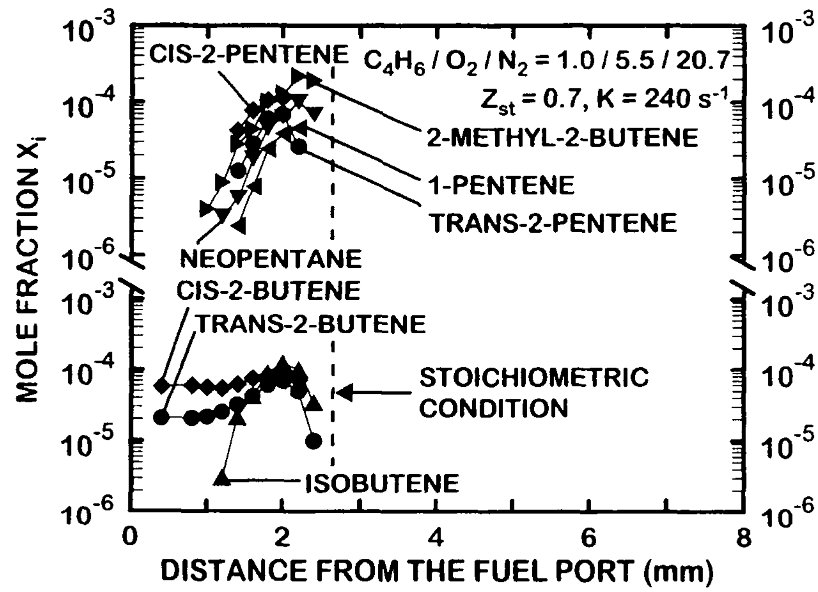

FIGURE 3 Measured minor gas species concentrations in a permanently-blue, 1,3-butadiene-fueled, diffusion flame at a strain rate of 240 s^{-1}.

a large number of intermediate hydrocarbon species are detected for fuel-rich conditions, extending up to C_6 hydrocarbons, which suggests complicated fuel-decomposition processes within the fuel-rich regions of the 1,3-butadiene-fueled diffusion flames. The similarity of the flame structure for various strain rates suggests the possible existence of state relationships for the 1,3-butadiene diffusion flames over the present range of strain rate variations. Similar to the propylene-fueled flames, the water vapor concentrations illustrated in Figure 2 were calculated without considering preferential-diffusion effects.

State Relationships

The measured flame structure data for the present propylene-fueled, permanently-blue, diffusion flames were correlated in order to determine whether state relationships existed for these flames over the present strain rate range. The resulting measured state relationships for the permanently-blue, propylene-fueled, diffusion flames are illustrated in Figures 4 and 5 for major and minor gas species, respectively. In these

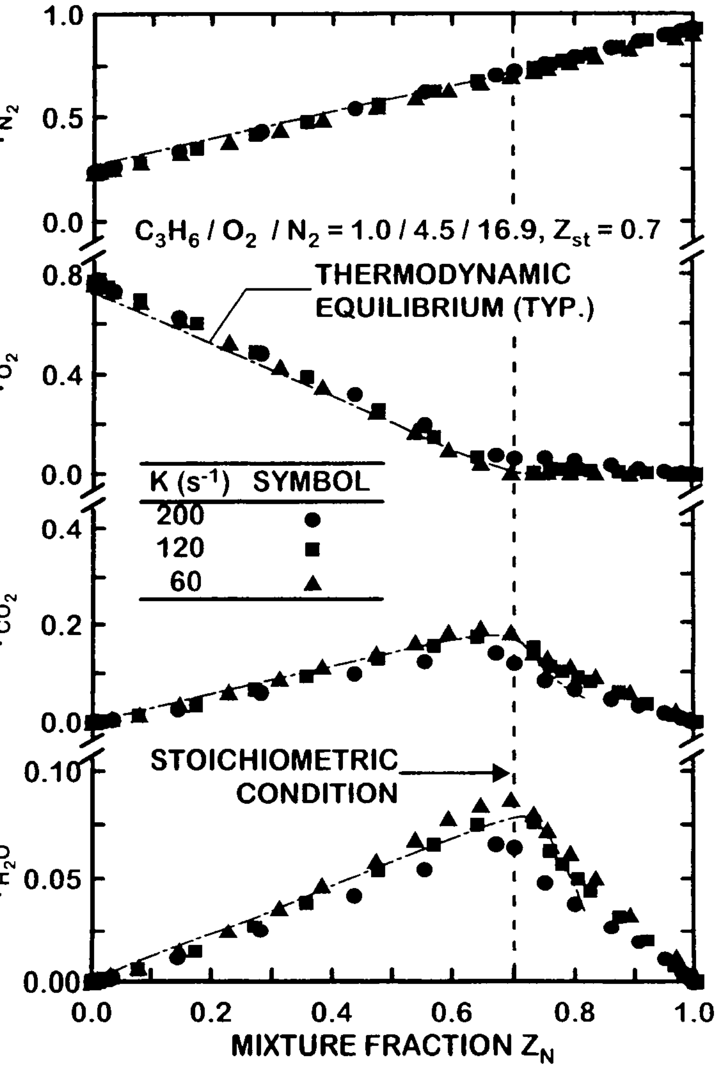

FIGURE 4 State relationships for N_2, O_2, CO_2 and H_2O concentrations for permanently-blue, propylene-fueled, diffusion flames

figures, the mass fractions of N_2, O_2, CO_2, H_2O, H_2, CO and C_3H_6, are plotted as a function of mixture fraction based on the nitrogen concentrations. On these figures, the measurements are represented by symbols while predictions based on the assumption of thermodynamic

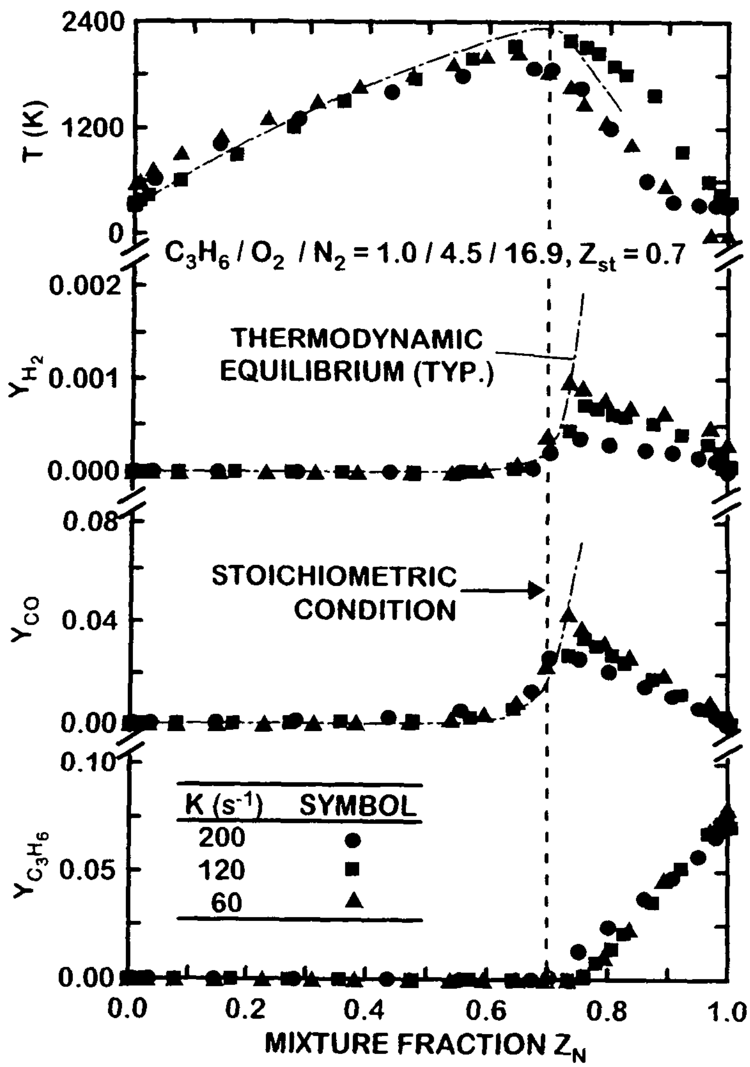

FIGURE 5 State relationships for temperatures and H_2, CO and fuel concentrations for permanently-blue, propylene-fueled, diffusion flames.

equilibrium using CEC computer code of Gordon and McBride (1971) are represented by lines. Note that the water vapor concentrations were estimated without considering preferential-diffusion effects due to lack of predictions of flame structure and are subject to adjustment given improved information about distributions of C/H molar ratios in these flames. The measured results correlate within experimental uncertainties as single universal curves for each gas species, suggesting the existence of state relationships for these permanently-blue propylene-fueled diffusion flames over the strain rate range of 0–200 s^{-1}, in spite of the complicated fuel decomposition processes for propylene. The results for gas temperatures and H_2 concentrations are less satisfactory: maximum temperatures tend to decrease as the strain rate increases due to effects of quenching and also decrease at low strain rates due to increased heat losses to the burner ports and due to radiation; H_2 concentrations seem to reflect an approach to quenching conditions as strain rates increase. The equilibrium predictions agree quite well with current measurements in the fuel-lean region but deviate from the measurements in the fuel-rich region due to finite rate reactions; this behavior is typical of past observations of state relationships in hydrocarbon-fueled diffusion flames burning in air (Lin and Faeth, 1998; Bilger, 1976; Sivathanu and Faeth, 1990).

Measured state relationships for major and minor gas species and gas temperatures for the permanently-blue 1,3-butadiene-fueled diffusion flames are illustrated in Figures 6 and 7 for strain rates of 60, 120 and 240 s^{-1}. In these two figures, the measurements are represented by symbols while the predictions by thermodynamic equilibrium using CEC computer code of Gordon and McBride (1971) are represented by lines. The water vapor concentrations were estimated without considering preferential-diffusion effects, as before. The measured results exhibit encouraging correlations for each gas species and gas temperatures within current range of strain rates, similar to results discussed in connection with Figures 4 and 5. This behavior supports use of the laminar flamelet concept without adjustment of state relationships for strain rate variations, to provide significant computational simplifications for modeling purposes in many instances. The general features of these correlations are similar to the permanently-blue ethylene- and propylene-fueled flames. Nitrogen yields a trivially good state relationship because mixture fractions are defined by nitrogen concentrations. Oxygen, carbon dioxide, carbon monoxide and fuel concentrations also exhibit reasonable universal state relationships for the present flames. Hydrogen and gas temperatures are less satisfactory due to the experimental uncertainties and effects of quenching and heat losses

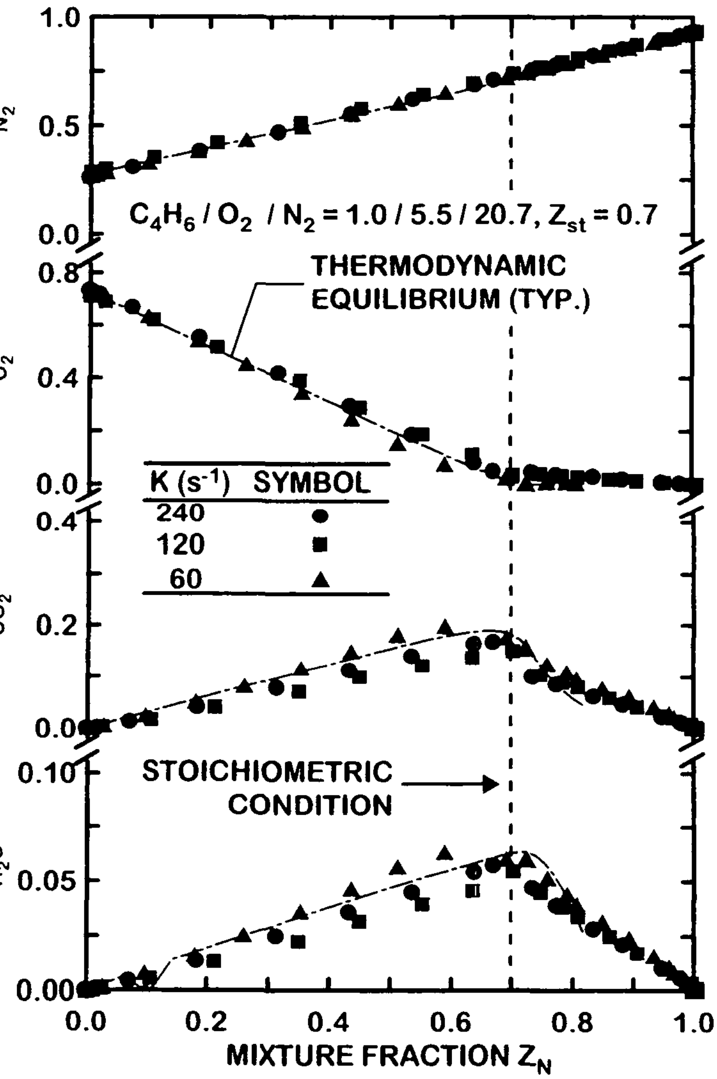

FIGURE 6 State relationships for N_2, O_2, CO_2 and H_2O concentrations for permanently-blue, 1,3-butadiene-fueled, diffusion flames.

on flow temperatures while the water vapor correlation is questionable and should be adjusted once predictions of C/H ratios are available so that corrections can be made for preferential-diffusion effects. Similar to the propylene-fueled diffusion flames, the predictions based on the

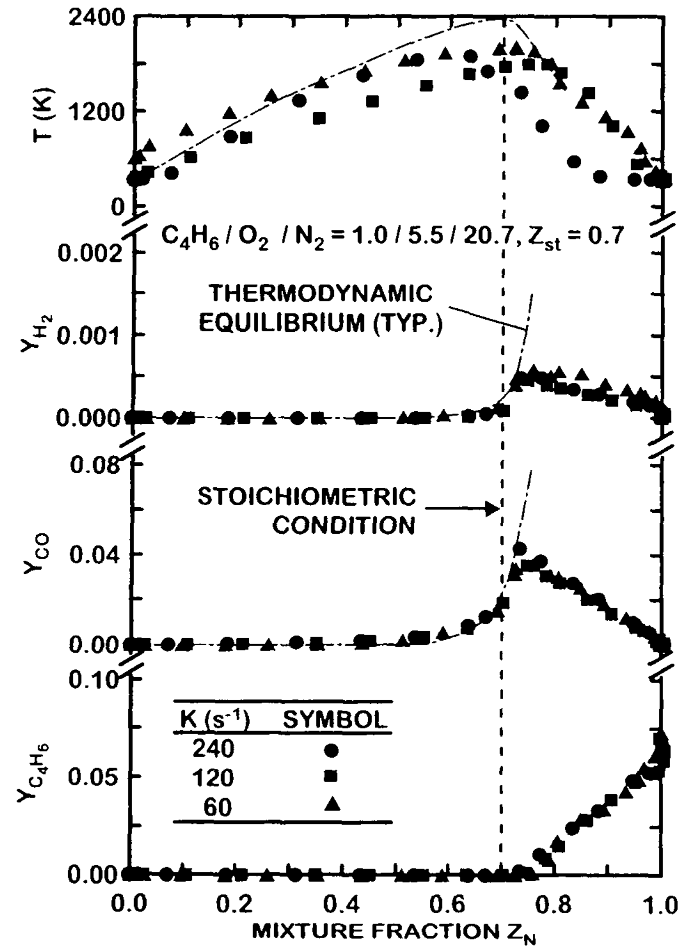

FIGURE 7 State relationships for temperature and H_2, CO and fuel concentrations for permanently-blue, 1,3-butadiene-fueled, diffusion flames.

assumption of thermodynamic equilibrium are in good agreement with the measurements in the fuel-lean region only.

Generalized State Relationships

The measurements of current propylene- and 1,3-butadiene diffusion flames, combined with both the measurements and predictions of ethylene-fueled diffusion flames from Lin and Faeth (1998), over the available range of strain rates, were collected as a data base to establish the effectiveness of the generalized state relationship functions summarized in Table I. The resulting generalized state relationships for the concentrations of N_2, H_2O, CO_2 and the temperature are plotted as a function of mixture fraction in Figure 8. As before, symbols indicate the measurements while

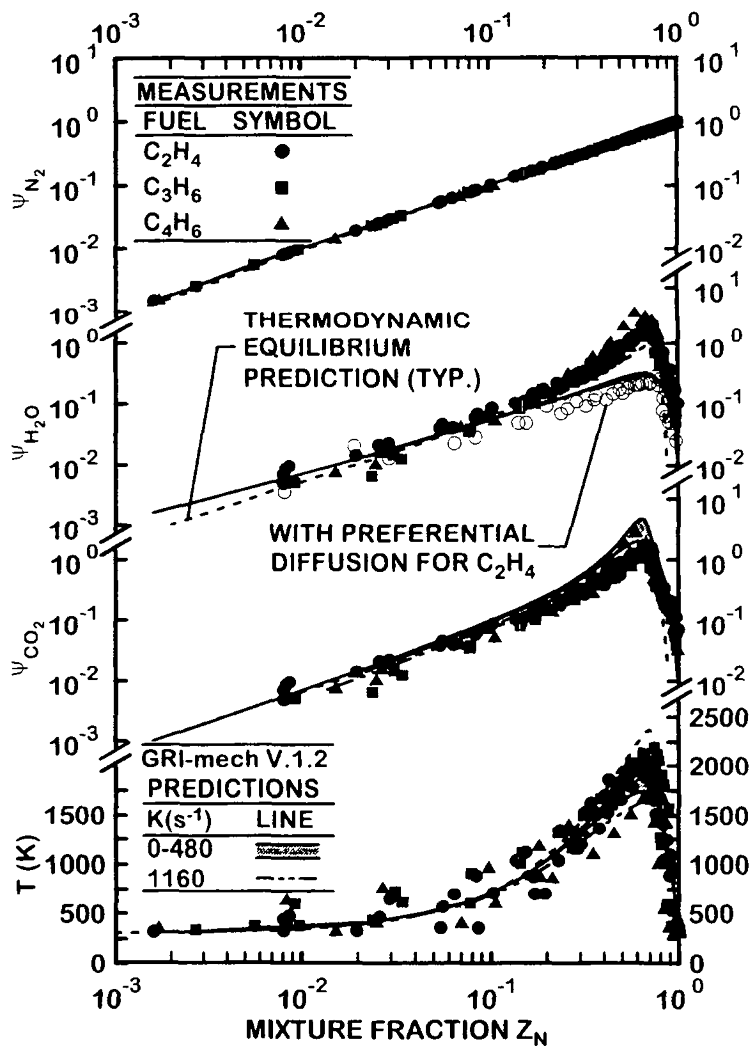

FIGURE 8 Generalized state relationships of temperature and N_2, CO_2 and H_2O concentrations for permanently-blue, hydrocarbon-fueled, diffusion flames.

lines indicate either numerical simulations (for ethylene) or the results of thermodynamic equilibrium calculations and mixture fractions were calculated based on nitrogen concentrations to avoid problems of preferential-diffusion effects. The nitrogen concentrations exhibit excellent generalized state relationships, which is trivial because mixture fractions have been based on nitrogen concentrations. The generalized state relationships of water vapor exhibit two different trends depending on the method used to calculated the water vapor concentrations. The water vapor concentrations calculated from preserved C/H molar ratios throughout the flames collapse into a single curve, and agree reasonably well with the thermodynamic equilibrium predictions for fuel-lean conditions. On the other hand, the water vapor concentrations calculated from the predicted C/H molar ratios, allowing for preferential-diffusion effects for ethylene-fueled diffusion flames, and represented by open symbols in Figure 8, yield another universal curve which is lower than the curve that is found by neglecting preferential-diffusion effects and matches reasonably well with the numerical predictions from Lin and Faeth (1998) using the Frenklach *et al.* (1995) and Peters (1993) mechanisms. Once again, direct measurements of water vapor concentrations are needed to resolve these differences. Measurements of CO_2 concentrations yield a reasonably good state relationship and agree quite well with the thermodynamic equilibrium predictions in the fuel-lean region. The predictions of CO_2 concentrations from Lin and Faeth (1998) using the Frenklach *et al.* (1995) and Peters (1993) mechanisms for the ethylene-fueled diffusion flames exhibit larger maximum values and a broader distribution range than the measurements, within a broad range of strain rates. The generalized state relationships for measured gas temperatures are less satisfactory than the rest because maximum temperatures vary from 1700 K to 2200 K. The predicted peak gas temperatures for ethylene-fueled diffusion flames, with strain rates varying from roughly zero up to near extinction conditions, also exhibit variations of state relationships. The peak gas temperatures predicted based on the assumption of thermodynamic equilibrium have the highest values, as expected.

The generalized state relationships for the concentrations of O_2, CO, H_2 and fuel are illustrated in Figure 9. The measurements and predictions of oxygen concentrations correlate quite well for fuel-lean conditions but exhibit some discrepancies for fuel-rich conditions. The measurements show that oxygen leaks into the fuel-rich region for the propylene-

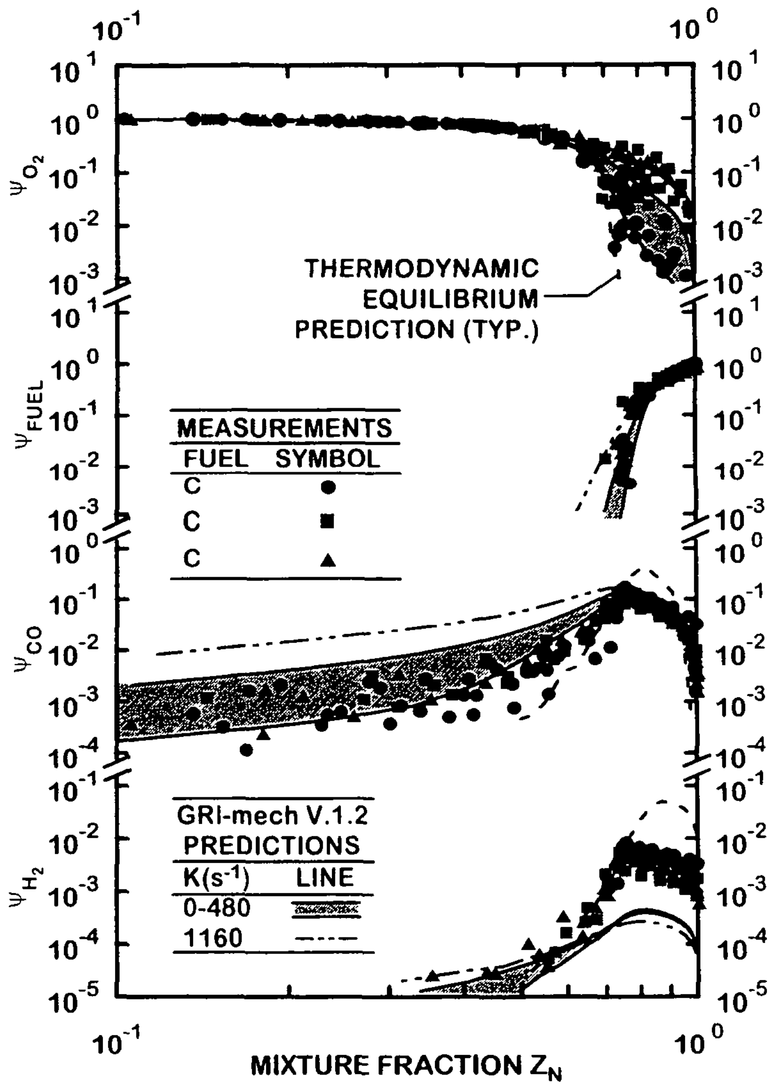

FIGURE 9 Generalized state relationships of O_2, fuel, CO and H_2 concentrations for permanently-blue, hydrocarbon-fueled, diffusion flames.

and 1,3-butadiene-fueled flames due to complicated, finite rate, fuel-decomposition processes. The scattering of the measurements may also result from increased experimental uncertainties at low species concentrations. The predictions of oxygen concentrations for the ethylene-fueled diffusion flames also correlate quite well as state relationships for fuel-lean conditions but exhibit variations due to varying strain rates in the fuel-rich region; large experimental uncertainties in this region due to small oxygen concentrations are a factor in this behavior. As Lin and Faeth (1998) observed, levels of oxygen leakage to fuel-rich conditions increase as the strain rates increase. Whether oxygen leakage to fuel-rich conditions for propylene- and 1,3-butadiene-fueled diffusion flames will further increase as strain rates increase must be examined once chemical reaction mechanisms are available for appropriate numerical simulations. The generalized state relationships for the fuels yield fair correlations in the fuel-rich region, but with slightly higher concentrations for 1,3-butadiene-fueled diffusion flames and near-extinguished ethylene-fueled flames. This behavior may also be caused by finite-rate chemistry for fuel-decomposition processes. In contrast to oxygen concentrations, however, carbon monoxide exhibits a very good generalized state relationship for fuel-rich conditions based on both measurements and predictions, except for the thermodynamic equilibrium calculation which predicts higher peak values. The measurements in the fuel-lean region, however, display obvious discrepancies from the predictions and a wide range of scattering. This can be explained by noting that the predictions of CO concentrations for ethylene-fueled diffusion flames show that CO concentrations are quite sensitive to the strain rate variations. As concluded by Lin and Faeth (1998), the main effect of increased strain rates is to cause increased levels of CO leakage to fuel-lean conditions. Both the measurements and the predictions suggest that the existence of generalized state relationships for CO in the fuel-lean condition is questionable. The generalized state relationship for H_2 is less satisfactory due the larger experimental uncertainties at the low concentrations of this species. The measurements of H_2 concentrations yield a fair correlation while the numerical simulations predict somewhat lower concentrations.

The main features of the generalized state relationships illustrated in Figures 8 and 9 can be summarized as follows: both measurements and predictions support relatively universal generalized state relationships for the concentrations of N_2, CO_2, H_2O and fuel over a broad range of strain rate and fuel type variations; effects of preferential diffusion must be resolved in order to obtain accurate results for H_2O concentrations; state relationships for O_2 in the fuel-rich region and CO in the fuel-lean region are functions of strain rate and fuel type; state relationships for H_2 and temperature exhibit less universality than other flame properties, probably due to measured experimental uncertainties for these variables. Nevertheless, the use of state relationships for scalars exhibiting significant effects of strain rates may still be useful in some instances, particularly when the strain rate range is limited, which is typical of practical flames.

CONCLUSIONS

The structure of permanently-blue propylene- and 1,3-butadiene-fueled diffusion flames at normal temperature and pressure was measured, considering various strain rates for the opposed-jet diffusion flame configuration. These results along with previous measurements and predictions for ethylene-fueled diffusion flames due to Lin and Faeth (1998) were used to develop state relationships for permanently-blue diffusion flames having a stoichiometric mixture fraction of 0.7. The main conclusions of the study are as follows:

1. Measured major gas species concentrations and temperature distributions of propylene- and 1,3-butadiene diffusion flames were similar to the measurements of ethylene-fueled diffusion flames due to Lin and Faeth (1998) over a range of strain rates. Based on earlier findings for the ethylene-fueled flames, direct measurements are needed to better quantify preferential-diffusion effects that significantly influence the distributions of water vapor concentrations.
2. Reasonably good measured state relationships for major gas species and gas temperatures were observed for propylene- and 1,3-butadiene diffusion flames over the present range of strain rates. These state relationships approximate thermodynamic equilibrium conditions at fuel-lean mixture ratios but depart from equilibrium conditions for fuel-rich mixture ratios due to effects of finite rate chemistry.
3. Generalized state relationships for major gas species were found for permanently-blue ethylene-, propylene- and 1,3-butadiene-fueled diffusion flames having stoichiometric mixture fractions of 0.7 for the current range of strain rates. The existence of these state relationships for permanently-blue hydrocarbon-fueled diffusion flames offers significant computational simplifications for modeling purposes in some instances.

NOMENCLATURE

a	number of moles of N_2 per mole of fuel in the fuel stream
b	number of moles of N_2 per mole of fuel in the oxidizer stream
f	fuel-stream to oxidizer-stream mass ratio
K	strain rate
k	number of moles of N_2 per mole of O_2 in the nonfuel gases, $k = 3.76$ for dry air
m	number of atoms of H in the fuel molecule
M_i	molecular weight of species i
n	number of atoms of C in the fuel molecule
T	temperature
v	streamwise velocity
X_i	mole fraction of species i
Y_i	mass fraction of species i
Z	mixture fraction
Z_{st}	stoichiometric mixture fraction

Greek Symbols

χ	molal oxidizer-stream to fuel-stream flow rate ratio
ϕ	fuel-equivalence ratio
ψ_i	generalized state relationship function for species i

Subscripts

f	fuel
F	initial property of fuel stream
O	initial property of oxidizer stream
S	stoichiometric condition
react	reactant mixture

Acknowledgment

This research was funded by the Office of Naval Research (Grant No. N00014-93-0321) under the technical management of G. D. Roy and by NASA (Grant Nos. NAG3-1245 and 2048) under the technical management of D. L. Urban.

References

Bilger, R W (1976). Turbulent jet diffusion flames. *Prog. Energy Combust. Sci.*, **1**, 87
Bilger, R. W. (1977). Reaction rates in diffusion flames. *Combust. Flame*, **30**, 277.

Du, J. and Axelbaum, R. L. (1995). The effect of flame structure on soot-particle inception in diffusion flames. *Combust. Flame*, **100**, 367.

Frenklach, M., Wang, H., Bowman, C. T., Hanson, R. K., Smith, G. P., Goldin, D. M., Gardiner, W. C. and Lissianski, V. (1995). World Wide Web Location http://www.gri.org/Basic Research/GRI-MECH

Fristrom, R. M. and Westenberg, A. A. (1965). *Flame Structure*, McGraw Hill Book Co., New York.

Gordon, S. and McBride, B. J. (1971). Computer program for calculation of complex chemical equilibrium compositions, rocket performance, incident and reflected shocks, and Chapman-Jouget detonations. NASA SP-273.

Kee, R. J., Miller, J. A., Evans, G. H. and Dixon-Lewis, G. (1988). A computational model of the structure and extinction of strained, opposed flow, premixed methane-air flames. In *Twenty-Second Symposium (International) on Combustion*, The Combustion Institute, Pittsburgh, pp. 1479–1494.

Lin, K.-C. (1996). Hydrodynamic effects on soot formation in laminar hydrocarbon-fueled diffusion flames. Ph.D. Thesis, The University of Michigan, Ann Arbor, Michigan.

Lin, K.-C. and Faeth, G. M (1996a). Hydrodynamic suppression of soot emissions in laminar diffusion flames *J Prop. Power*, **12**, 10.

Lin, K.-C. and Faeth, G. M. (1996b). Effects of hydrodynamics on soot formation in laminar opposed-jet diffusion flames. *J Prop Power*, **12**, 691.

Lin, K C. and Faeth, G. M (1998) Structure of laminar permanently-blue opposed-jet ethylene-fueled diffusion flames *Combust. Flame*, **115**, 468.

Lin, K.-C., Sunderland, P. B and Faeth, G. M. (1996). Soot nucleation and growth in acetylene/air laminar coflowing jet diffusion flames *Combust. Flame*, **104**, 369.

Mitchell, R. E., Sarofim, A. F and Clomburg, L. A (1980). Experimental and numerical investigation of confined laminar diffusion flames *Combust. Flame*, **37**, 227.

Peters, N. (1993). Flame calculations with reduced mechanisms — an outline. In Peters, N. and Rogg, B. (Eds.), *Reduced Kinetic Mechanisms for Applications in Combustion Systems*, Springer-Verlag, Germany, pp. 3–14.

Saito, K., Williams, F. A. and Gordon, A. S. (1986). Structure of laminar coflow methane-air diffusion flames *J Heat Trans.*, **108**, 640.

Seshadri, K. and Williams, F. A. (1978) Laminar flow between parallel plates with injection of a reactant at high Reynolds number. *Int. J. Heat Mass Trans.*, **21**, 251.

Sivathanu, Y. R. and Faeth, G. M. (1990) Generalized state relationships for scalar properties in nonpremixed hydrocarbon/air flames. *Combust Flame*, **82**, 211.

Smyth, K. C., Miller, J H., Dorfman, R. C., Mallard, W. G. and Santoro, R. J. (1985). Soot inception in a methane/air diffusion flame as characterized by detailed species profiles. *Combust. Flame*, **62**, 157.

Sugiyama, G. (1994). Nonluminous diffusion flame of diluted acetylene in oxygen enriched air. In *Twenty-Fifth Symposium (International) on Combustion*, The Combustion Institute, Pittsburgh, PA, pp. 601–608.

Sun, C J., Sung, C. J., Wang, H. and Law, C. K. (1996). On the structure of non-sooting counterflow ethylene and acetylene diffusion flames. *Combust. Flame*, **107**, 321.

Sunderland, P B, Köylu, U. Ö and Faeth, G. M. (1995). Soot formation in weakly-buoyant acetylene-fueled laminar jet diffusion flames burning in air. *Combust. Flame*, **100**, 310.